SCIENTIFIC REPORTS

OPEN

SUBJECT AREAS:
X-RAY CRYSTALLOGRAPHY
INTRINSICALLY DISORDERED PROTEINS
LEARNING AND MEMORY
STRUCTURE DETERMINATION

Received
13 October 2012

Accepted
21 February 2013

Published
6 March 2013

Correspondence and requests for materials should be addressed to J.S. (dbsjayar@nus.edu.sg)

Structural Basis for the Interaction of Unstructured Neuron Specific Substrates Neuromodulin and Neurogranin with Calmodulin

Veerendra Kumar[1], Vishnu Priyanka Reddy Chichili[1], Ling Zhong[4], Xuhua Tang[1], Adrian Velazquez-Campoy[5], Fwu-Shan Sheu[2], J. Seetharaman[3], Nashaat Z. Gerges[4] & J. Sivaraman[1]

[1]Department of Biological Sciences, National University of Singapore, Singapore, 117543, [2]NUSNNI-NanoCore, National University of Singapore, T-Lab Level 11, 5A Engineering Drive 1, Singapore 117580, [3]X4 Beamline, Brookhaven National Laboratory, Upton, New York, US, [4]Department of Cell Biology, Neurobiology and Anatomy, Medical College of Wisconsin, Milwaukee, WI 53226 0509, USA, [5]Department of Biochemistry and Molecular and Cell Biology, Institute of Biocomputation and Physics of Complex Systems (BIFI), Unidad Asociada IQFR-CSIC-BIFI, Universidad de Zaragoza, Spain, and Fundacion ARAID, Diputacion General de Aragon, Spain.

Neuromodulin (Nm) and neurogranin (Ng) are neuron-specific substrates of protein kinase C (PKC). Their interactions with Calmodulin (CaM) are crucial for learning and memory formation in neurons. Here, we report the structure of IQ peptides (24aa) of Nm/Ng complexed with CaM and their functional studies with full-length proteins. Nm/Ng and their respective IQ peptides are intrinsically unstructured; however, upon binding with CaM, IQ motifs adopt a helical conformation. Ser41 (Ser36) of Nm (Ng) is located in a negatively charged pocket in the *apo* CaM and, when phosphorylated, it will repel Nm/Ng from CaM. These observations explain the mechanism by which PKC-induced Ser phosphorylation blocks the association of Nm/Ng with CaM and interrupts several learning- and memory-associated functions. Moreover, the present study identified Arg as a key CaM interacting residue from Nm/Ng. This residue is crucial for CaM-mediated function, as evidenced by the inability of the Ng mutant (Arg-to-Ala) to potentiate synaptic transmission in CA1 hippocampal neurons.

Neuromodulin (Nm) and neurogranin (Ng) are neuron-specific substrate proteins belonging to the calpacitin protein family[1–3]. Nm and Ng share high sequence similarity spanning a 20-amino-acid region that contains an IQ motif (I/L/V)QXXXRXXXX(R/K). Both proteins bind to Calmodulin (CaM) through this IQ motif under a low Ca^{2+} micro-environment and dissociate when Ca^{2+} levels increase[1,2]. In resting neurons, much of the CaM is associated with Nm/Ng in the membrane[4].

Nm is a 23.6 kDa protein localized at the cytoplasmic face of the plasma membrane in the presynaptic terminals of axons. During neural development, Nm accumulates in axonal growth cones and helps their navigation toward appropriate target sites[5]. In addition, Nm is involved in neurite extension and neuronal plasticity, neuroregeneration, regulation of neurotransmitter release at the presynaptic terminal, and in the long-term potentiation (LTP) of synaptic efficiency[6]. In the nervous system, Nm becomes phosphorylated during LTP in the hippocampal area, CA1[7]. Further, Nm contributes to synaptic plasticity by controlling the levels of presynaptically available CaM[4,8]. Overexpression of Nm is accompanied by enhanced learning and regenerative capabilities[9], with recent studies suggesting that protein kinase C (PKC)-induced phosphorylation of Nm differentially regulates the performance of three diverse memory-associated tasks[10].

Ng, on the other hand, is a 7.6 kDa protein that is expressed at postsynaptic cytosol loci in several telencephalic areas in mammals, such as the cerebral cortex, hippocampus, amygdala, striatum and olfactory bulb[2]. Its expression is controlled by thyroid hormone[11], and vitamin A[12], and is developmentally regulated, with relatively low levels of expression observed in the embryonic and neonatal stages followed by dramatic increases from about 2–3 weeks of age in the rodent brain[13]. While Ng enhances synaptic strength through its interaction with CaM[14], Ser36 phosphorylation renders Ng unable to bind to either CaM or phosphatidic acid[15,16]. Ng knockout strongly diminishes the LTP and slightly enhances long-term depression (LTD)[17]. Similar to Nm, Ng plays an important

role in the neuroplasticity mechanism of learning and memory. Ng mutants that lack the ability to bind to CaM, or dissociate from CaM, are unable to potentiate synaptic transmissions, strongly suggesting that regulated Ng-CaM binding is necessary for Ng-mediated potentiation[18,19].

In combination with a review of the literature, the present study has revealed that Nm and Ng are intrinsically unstructured proteins (IUP) under *in-vitro* physiological conditions[1]. These proteins have very little or no secondary structure and lack a compact globular fold. Moreover, previous studies have revealed that Nm and Ng interact with CaM through their IQ motifs, which assume an α-helical structure upon binding to CaM[20–24]. To gain insight into the specific recognition of CaM by these intrinsically unstructured proteins, we investigated the biophysical interactions and structure of Nm/Ng and IQ motif peptides in association with CaM. Besides, the functional studies were performed to validate our findings.

Results

Nm and Ng are intrinsically unstructured proteins. *Residual secondary structure from far UV-CD.* CD spectra of Nm and Ng showed an intense minimum at 201 and 204 nm respectively, indicating the presence of disordered regions in these proteins. The CD analysis further supports that Nm and Ng both have residual secondary structural elements (mainly α-helix) and suggests that these two proteins exist in a premolten globular conformational state of protein quartet model[25] under physiological conditions (Supplementary Figure 2A) .

NMR spectroscopy suggests Nm and Ng are natively unfolded proteins. ^{1}H NMR is a sensitive method capable of distinguishing between folded and unfolded proteins through a small dispersion of the amide backbone chemical shift[26]. Particularly, the appearance of a large and broad signal at approximately 8.3 ppm is an indicator for a disordered protein. On the other hand, signal dispersion beyond 8.5 ppm (8.5–11 ppm) indicates a folded protein. Further, in the aliphatic region of the ^{1}H NMR spectrum between +1.0 and −1.0 ppm, large-signal dispersion versus a steep flank of the dominant peak at approximately 1.0 ppm will separate a structured protein from an unfolded protein[26]. The NMR spectra of full-length Nm and Ng were very similar to those previously observed for other unstructured proteins (Supplementary Figures 2B and 2C). The resonance of both protein's methyl group protons (at 0.9 and 0.95 ppm) and amide groups (around 8.4 ppm), along with very limited spectral dispersion of these signals, indicated the lack of a stable tertiary structure in both Nm and Ng (Supplementary Figures 2B and 2C). The observed intense H-alpha peaks might be due to 1) a reduced exchange of H-alpha with D_2O[26] in the sample; and 2) the unstructured nature of these two proteins[1].

Nm and Ng have a low percentage of order-promoting amino acids and high percentage of disorder-promoting amino acids (Supplementary table 1). The acidic pI and low hydrophobicity of these two proteins indicates that they are unfolded (See supplementary text). Besides, gel filtration chromatography and Dynamic Light Scattering experiments show the higher hydrodynamic radii and molecular weight for both Nm and Ng (See supplementary text). Thus, the biophysical studies on Nm and Ng support the classification of these proteins as intrinsically unstructured, lacking a compact globular fold, and having very little secondary structure[27–29].

Isothermal titration calorimetry. The sequence alignment of known CaM binding peptides showed that each has one or two key aromatic residues, a few basic amino acids (located at N or C terminal) and other hydrophobic amino acids (Figure 1). Nm and Ng protein sequences do not have any aromatic residues at the N-terminal region of the IQ motif. However, both IQ motifs are enriched with basic amino acids in the C-terminal region. Based on the sequence alignment, we selected peptides surrounding the IQ motif for Nm (NmIQ) and Ng (NgIQ) in order to mimic the interactions of their full-length counterparts with CaM. The ITC experiments were performed with full-length Nm/Ng proteins and IQ peptides with CaM (Table 1 and Figure 2).

ITC experiments revealed that the full-length Nm and Ng bind to *apo* CaM (in the absence of Ca^{2+}) with a higher affinity than that to Ca^{2+}/CaM. These observations are consistent with the previous fluorescence experiments[1] (Table 1). Further, the ITC results show that NmIQ and NgIQ peptides have a similar affinity toward *apo* CaM as their full-length counterparts; thus, the IQ peptides almost mimic their full-length proteins. Nm and Ng interacted with CaM mainly through their IQ motifs with a stoichiometric ratio of 1 : 1.

Nm/Ng CaM complex structural studies. The Nm and Ng are intrinsically unstructured proteins. Brief attempts to crystallize the full-length Nm and Ng alone and in complex with *apo* and Ca^{2+}/CaM did not yield crystals. This led us to crystallize the IQ motif peptides in complex with CaM instead. Initially, we attempted to co-crystallize the synthetic IQ motif peptides with *apo* CaM and Ca^{2+}/CaM; however no complex crystals were obtained. Our previous and current NMR studies have shown that the complex formation between Ng and CaM is not very stable[20]. In order to circumvent this problem, based on the CaM structure analysis and literature, the IQ peptides were linked with CaM via a $(Gly)_5$ linker[30].

NmIQ and NgIQ, both 24aa peptides, were linked to the C-terminal of CaM through a 5-aa Gly linker (referred to as *apo*

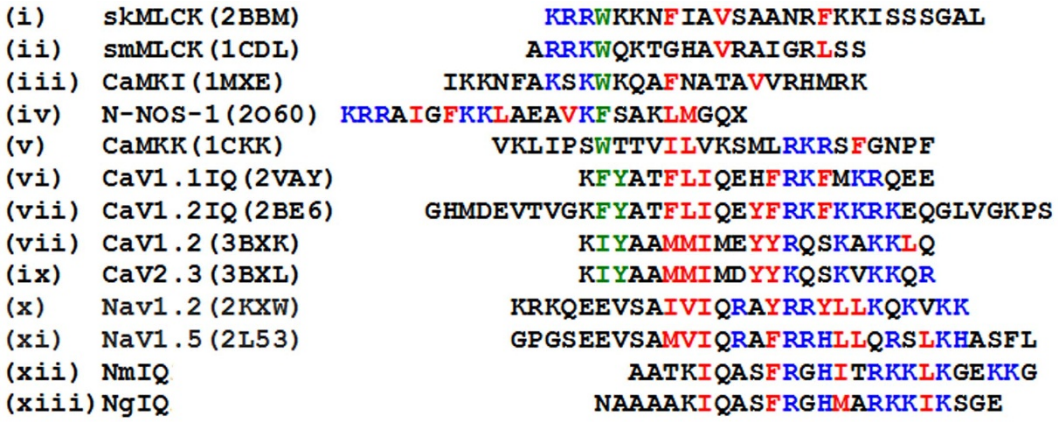

Figure 1 | Structure-based sequence alignment of CaM binding peptides from different proteins. Sequence analysis shows a critical aromatic amino acid (green) that anchors the peptide into CaM; a positively charged amino acid (blue) that determines the orientation of the peptide between two lobes of CaM; and hydrophobic amino acids (red) that are involved in binding. The pdb codes are given in parentheses.

Table 1 | Association constant (K_a) for the interaction of Nm/Ng proteins and peptides with CaM

		K_a (10^6 M^{-1})
Nm_{WT}	apoCaM	7.9
	Ca^{2+}/CaM	0.52
Ng_{WT}	apoCaM	23
	Ca^{2+}/CaM	0.96
NmIQ	apoCaM	25
	Ca^{2+}/CaM	1.6
NgIQ	apoCaM	2.3
	Ca^{2+}/CaM	0.3
Nm_{WT}	CaM_{D81A}	5.0
	CaM_{E85A}	3.5
	CaM_{F142A}	1.4
	$CaM_{E85A/F142A}$	0.46
CaM_{WT}	Nm_{F42A}	Null
	Nm_{R43A}	Null
	Nm_{I46A}	Null
Ng_{WT}	CaM_{F90A}	0.80
	CaM_{E115A}	1.2
	CaM_{E121A}	3.1
	CaM_{M125A}	3.7
	$CaM_{F90A/E121A}$	Null
CaM_{WT}	Ng_{I33A}	Null
	Ng_{Q34A}	Null
	Ng_{F37A}	Null
	Ng_{R38A}	Null

CaM-$(Gly)_5$-NmIQ and *apo* CaM-$(Gly)_5$-NgIQ), crystallized, and their structure independently solved by Single wavelength Anomalous Dispersion (SAD) method. Both models were refined up to 2.7 Å resolution, with good stereochemical parameters (Table 2). The *apo* CaM-$(Gly)_5$-NmIQ has two molecules in the asymmetric unit, whereas *apo* CaM-$(Gly)_5$-NgIQ has one molecule in the asymmetric unit. CaM in both structures existed in an extended conformation, with peptide binding to the C-lobe. The structures of both complexes were different (rmsd 4.1Å for 122 Cα atoms), where the Nm complex was in an open conformation and the Ng complex in a closed conformation. However, the C-lobe alone from both CaM structures superimposed with an rmsd of 2.1 Å (Figure 5). The bound peptides were well defined in the electron density map (Figure 3) and the models showed good geometry. No density was observed for the linker $(Gly)_5$ or for any metal ion in any of the divalent metal ion binding sites.

The amino acid distribution of CaM made the C-lobe more negatively charged than the N-lobe[31]. Notably, the NmIQ/NgIQ peptides lacked key, bulky hydrophobic residues, but were rich in positively charged amino acids (Figure 1). The crystal structure revealed that the bound NmIQ/NgIQ peptide adopted an α-helical structure that was almost perpendicular to the central α-helix of CaM, making several contacts with the C-lobe and a few contacts with central helix of CaM (Figure 3 and 4).

apo CaM-$(Gly)_5$-NmIQ. Residues Lys55-Gly57 of the NmIQ peptide were not well-defined in the electron density map and were not included in the model (Figure 3C). The PKC phosphorylation site Ser41 of NmIQ was in contact with Glu115 of CaM, residing in a negatively charged pocket consisting of Asp119, Glu120 and Glu121 of CaM (Figure 4A). Further, Arg43 of the NmIQ peptide made several contacts with the residues of the central helix of CaM, such as Glu85, Asp81 and Ser82 (Figure 4A). Other residues, such as Ile38, Gln39, Phe42 and Arg43, anchored the NmIQ peptide into a groove formed by the central helix and EF-motifs of CaM.

apo CaM-$(Gly)_5$-NgIQ. Similar to the *apo* CaM-$(Gly)_5$-NmIQ complex, the CaM in *apo* CaM-$(Gly)_5$-NgIQ complex existed in an extended conformation (Figure 3B). No electron density was observed for the loop between Met52 and Gly62 of CaM and for the last two residues (Gly49 and Glu50) of NgIQ (Figure 3D); these residues were not included in the model. Interestingly, the CaM interacting peptide of Ng was from the nearest symmetry-related molecule (Supplementary Figure 3) and the bound peptide was in the opposite direction to that observed in the CaM-$(Gly)_5$-NmIQ complex (Figure 5).

The N-terminal part of the peptide was deeply buried in a cleft formed by the helices from the EF-motif of CaM. The conserved residues of the IQ motif [(I/L/V)QXXXRXXXX(R/K)] interacted with CaM and anchored the Ng molecule (Figure 4B). Studies have previously shown that the Ser36-phosphorylated Ng is unable to bind CaM and phosphatidic acid[15,16]. In the *apo* CaM-$(Gly)_5$-NgIQ structure, Ser36 was buried in a pocket surrounded by negatively charged residues, such as Glu83, Glu84, Glu85 and Glu88 (Figure 4B).

To validate the structural findings, we carried out a structure-based mutation analysis on Nm, Ng and CaM to further study the interaction (Table 1). A single point substitution in Nm/Ng resulted in a complete loss in binding, while substitutions in CaM resulted in weakened binding (Table 1). On the other hand, interactions from the amino acids of CaM were dependent on their location.

Role of central Arg residues of IQ motifs. The IQ domain is approximately 25 amino acids in length and is widely distributed in nature. While the consensus sequence of IQ motif [(I/L/V)QXXXRXXXX(R/K)] is not strictly conserved, the central Arg (Arg43 in Nm and Arg38 in Ng) residue is highly conserved (Figure 1). The strictly conserved Arg might have an essential role in mediating the interaction of IQ motifs with CaM. In both the crystal structures, the Arg is surrounded by the highly negatively charged residues of CaM. An Arg to Ala point mutation resulted in a complete loss of binding. However, in the case of Ng, the Arg38Gln point mutation was shown to reduce the binding strength[23]. We have investigated the role of Arg to potentiate the synaptic transmission.

NgR38A cannot potentiate synaptic transmission. The role of Ng in postsynaptic function at CA1 hippocampal synapses has been well characterized. We have previously shown that overexpression of wild-type Ng potentiates synaptic transmission[19]. Ng-mediated enhancement of synaptic transmission is dependent on the regulated binding to CaM[19]. Here, we sought to test the effect of the mutant Arg38Ala on Ng binding to CaM and its effects on synaptic function. To verify this, we expressed a GFP-tagged NgR38A using the biolistic delivery method[32] in CA1 hippocampal neurons. After 12-15 hours of expression, α-amino-3-hydroxy-5-methyl-4-isoxazolepropionic acid receptor (AMPAR)- and *N*-methyl-d-aspartate receptor (NMDAR)-mediated responses from control and infected neurons were evaluated by double whole-cell patch clamping. As shown in Figure 6, NgR38A was unable to potentiate synaptic transmission. This is consistent with results from Ng mutants that cannot bind CaM or lack the IQ CaM binding site[19]. Besides, the Ng mutant R38A did not affect NMDAR-mediated responses. Collectively, these data support previous findings that Ng-CaM interaction is required for Ng-mediated enhancement of synaptic strength but is not essential in maintaining synaptic transmission.

Discussion

Nm and Ng have been the subjects of intense study for their potential roles in brain development and neural plasticity[8–10,19]. Both proteins are members of the calpacitin family and share a conserved IQ motif that mediates interactions among Ca^{2+}, CaM, and PKC signalling pathways[21,24,33]. PKC phosphorylates Ser41 (Nm) and Ser36 (Ng)

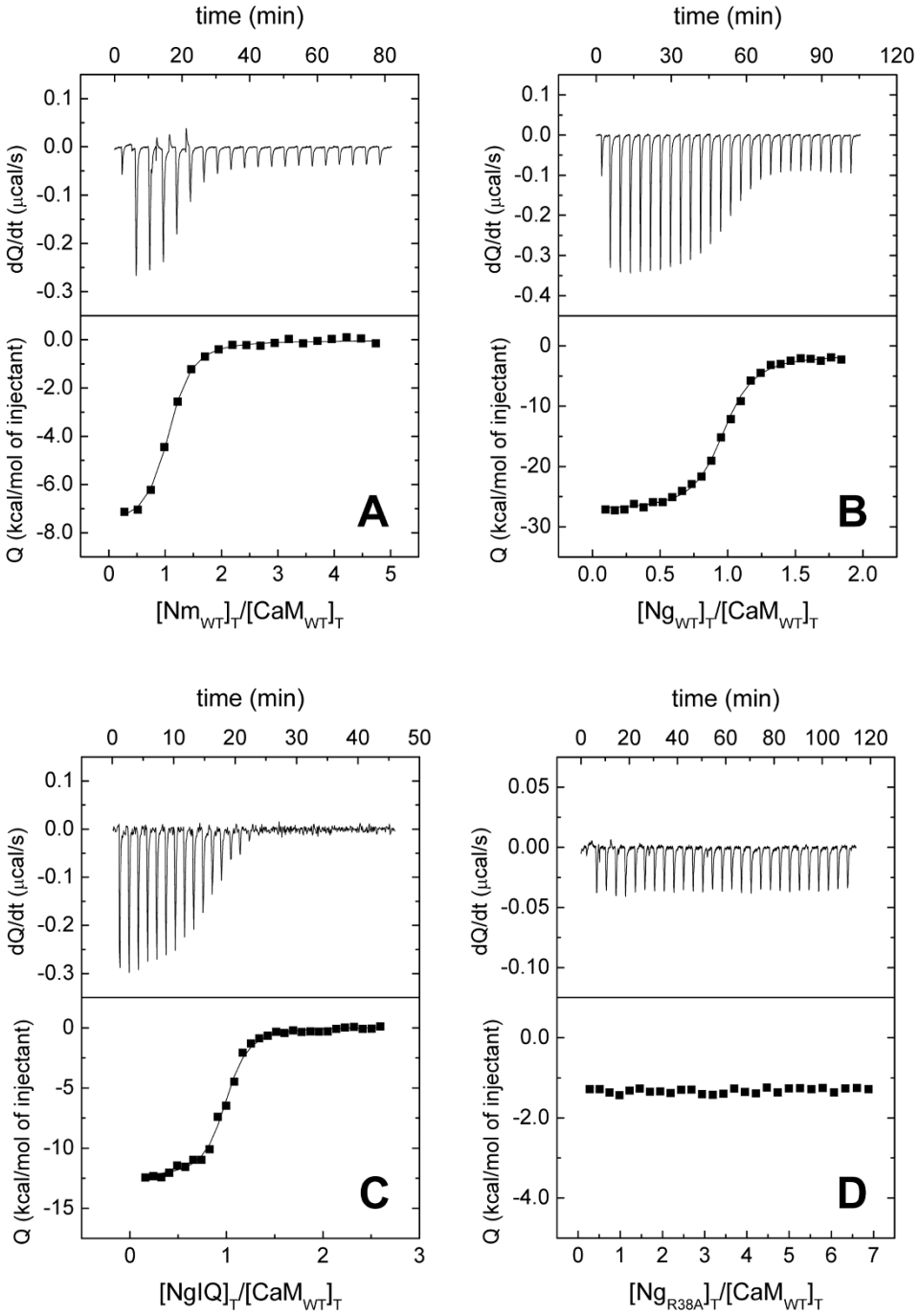

Figure 2 | Nm/Ng proteins and peptides interacting with CaM. ITC experiments corresponding to (A) Nm (B) Ng (C) NgIQ and (D) Ng_{R38A} titrated against *apo*CaM. Upper panels show the raw thermogram data; lower panels show the heat release for each injection (binding isotherm). The data have been fitted using a single-site binding model.

within the IQ motif, and when phosphorylated, these proteins are unable to bind CaM, which interrupts several learning- and memory-associated functions[8,10,16]. It has been shown that Ser36-phosphorylated Ng is unable to enhance synaptic strength[18,19,34]. Similarly, a separate study shows that genetically overexpressed wild-type Nm can enhance the learning and LTP in transgenic mice; but the over-expressed mutant Nm (S41A) does not[9]. Others have shown that interactions between a S41A Nm mutant and CaM in PC12B cells renders the interaction insensitive to Ca^{2+} concentrations *in vitro*, with the mutation inhibiting the association of Nm with the membrane skeleton of PC12B cells[35]. These findings suggest that the Ser41/Ser36 (Nm/Ng) phosphorylation sites are the main targets for enhancing cognitive ability.

In the complex crystal structure, the PKC phosphorylation sites, Ser41 and Ser36 of Nm and Ng, respectively, are completely surrounded by negatively charged amino acids (Figure 4). Consequently, the phosphorylation of this Ser residue will repel Nm/Ng from CaM due to electrostatic repulsion and steric hindrance. This explains why the phosphorylation of Ser by PKC blocks the Nm/Ng association with CaM and interrupts several learning- and memory-associated functions[8–10,18,21,34,35].

One proposed biochemical function of Nm and Ng is to target CaM at the membrane in the vicinity of 'CaM-activated enzymes' under low Ca^{2+} conditions at the pre- and post-synaptic terminals, respectively[1,22,24]. Therefore, Nm and Ng might serve as a Ca^{2+}-regulated modulators of CaM activity in neurons. Moreover, the strict

Table 2 | Crystallographic data and refinement statistics

	apo CaM-$(Gly)_5$-NmIQ		*apo* CaM-$(Gly)_5$-NgIQ	
	Peak	Native	Inflection	Peak
Cell parameters (Å, °)	a = 56.30, b = 56.40, c = 135.80, β = 90.76	a = 79.38, b = 79.28, c = 136.06, β = 90.19	a = 76.57, b = 76.57, c = 46.99	a = 76.46, b = 76.46, c = 46.95
Space group	P2	C2	$P4_1$	$P4_1$
Data collection				
Resolution range (Å) *	50.00–3.00 (3.11–3.00)	50.00–2.65(2.74–2.65)	30–2.70 (2.80–2.70)	30.00–2.60 (2.69–2.60)
Wavelength (Å)	0.978	1.541	0.964	0.979
Observed reflections >1σ	77387	105895	38257	157832
Unique reflections	31242(2393)	23563(2086)	7588(742)	8503(779)
Completeness (%)	93.4 (71.6)	95.2(85.5)	100(99.6)	98.9(92.8)
Overall (I/σ (I))	15.8(5.5)	24.7(3.7)	44.6(2.7)	18.8(2.0)
R_{sym}[a] (%)	9.5(18.3)	7.3(22.5)	7.2(42.8)	12.7(33.3)
Refinement and quality [b]				
Resolution range (Å)		30.0–2.69		30.00–2.70
R_{work}[c] (no. of reflections)		0.265 (21094)		0.24(7200)
R_{free}[d] (no. of reflections)		0.30(1278)		0.27(359)
RMSD bond lengths (Å)		0.007		0.012
RMSD bond angles(°)		1.12		1.43
Average B-factorse ($Å^2$)				
Main chain		56.8		61.6
Side chain		57.4		62.6
Ramachandran plot				
Most favored regions (%)		84.6		89.4
Additional allowed regions (%)		14.8		9.2
Generously allowed regions (%)		0.7		0.7
Disallowed regions (%)		0.0		0.7

[a]$R_{sym} = \sum |I_i - <I>| / |I_i|$ where I_i is the intensity of the ith measurement, and <I> is the mean intensity for that reflection.
[b]Reflections with I>σ was used in the refinement.
[c]$R_{work} = |F_{obs} - F_{calc}| / |F_{obs}|$ where F_{calc} and F_{obs} are the calculated and observed structure factor amplitudes, respectively.
[d]R_{free} = as for R_{work}, but for 5–7% of the total reflections chosen at random and omitted from refinement.
[e]Individual B-factor refinements were calculated.
*The high resolution bin details are in the parenthesis.

conservation of the region containing the IQ motif in all vertebrates suggests that both the PKC phosphorylation site and the CaM binding feature are essential to the functions of Nm and Ng[3]. Although the functions of Nm and Ng have been well established, the intrinsically unstructured nature of these two proteins, and the consequential lack of structural information, has seriously hampered a complete understanding of the interaction between Nm/Ng and CaM.

Moreover, the results from our study show that once the Nm/Ng binds to CaM, the interacting IQ motif regions of Nm/Ng become structured and adopt an α-helical conformation (Figure 3). Similar conformational changes of intrinsically unstructured binding partners of CaM have been shown for chicken gizzard caldesmon via physico-chemical experiments[27] and for PEP-19[28] and calponin[36] *via* NMR. Further, a previous NMR study reported a helical structure for the activation domain of CITED2, which is unstructured in its free form, in complex with its partner TAZ1[29]. The present report on the Nm/Ng with CaM is the first crystal structure of any neuron-specific intrinsically unstructured protein complexed with its binding partner. The C-lobe of CaM bound to the NgIQ peptide adopts semi-open conformation similar to that observed in the case of *apo* CaM bound to the first two IQ motifs of the murine myosin V heavy chain[37]. However, CaM bound to the NmIQ peptides was observed to be in an open conformation despite the absence of Ca^{2+} ions in any of the EF-hand motifs. Besides the IQ motif, Nm and Ng share no sequence homology. However, the N-terminal domain of both proteins is highly conserved among vertebrates, and the structural information provided here might be extended to other homologs.

The fragment Arg43-Leu51 of Nm has been reported to bind CaM-Sepharose both in the presence of Ca^{2+} or in an excess of EGTA, and can be eluted with 150 mM KCl[22]. However, the fragment Gln39-Lys55 (Trp substituted for Phe42) binding to CaM-Sepharose becomes Ca^{2+}-sensitive[22]. Phe42 of Nm interacts with CaM hydrophobically, and an increase in hydrophobicity at this position (Phe-to-Trp substitution) increases the Nm-CaM affinity by 10-fold[21]. The present crystal structure showed that the fragment Ile38-Phe42 of Nm is in the vicinity of the EF-motifs (i.e., a Ca^{2+}-binding site) of CaM (Figure 3A and Figure 4A). Thus, the binding of fragment Ile38-Phe42 (hence, Gln39-Lys55) is affected by binding of Ca^{2+} to the EF-motif. However, the Arg43-Leu51 fragment (mainly basic amino acids) binds through electrostatic interactions near the central helix of CaM, away from the EF-motifs, and thus remains insensitive to Ca^{2+}.

The identified key CaM interacting residues of NgIQ (Ile33, Ser36 and Arg38) are consistent with the residues identified in the full-length Ng for *in vivo* CaM binding[23]. The Ile33Gln (I33Q) point mutation completely inhibits the binding, while Ser36Asp (S36D) and Arg38Gln (R38Q) mutations reduce Ng-CaM binding[23]. In the crystal structure, Ile33 (of Ng) is a part of the strong hydrophobic cluster (Figure 4B). A point mutation at this position with a non-hydrophobic amino acid (e.g. I33Q) disrupts the hydrophobic interaction, creates steric hindrances, and abolishes the interaction between Ng and CaM[23]. Moreover, a point mutation of S36D in Ng would add a negative charge to this position, but cause less of an effect than if it were to be phosphorylated on Ser36[23]; i.e., while a S36D mutation will reduce Ng-CaM binding, a phosphorylation event will completely abolish it. Similarly, Arg38 of Ng makes hydrogen bonding contacts with Glu115 and Glu121 of CaM (Figure 4B). While the mutant Arg38Gln will reduce the binding, Arg38Ala will completely abolish (see above) the interaction.

In some cases, linking two proteins with a linker to retain the natural binding between the partners as an intramolecular interaction

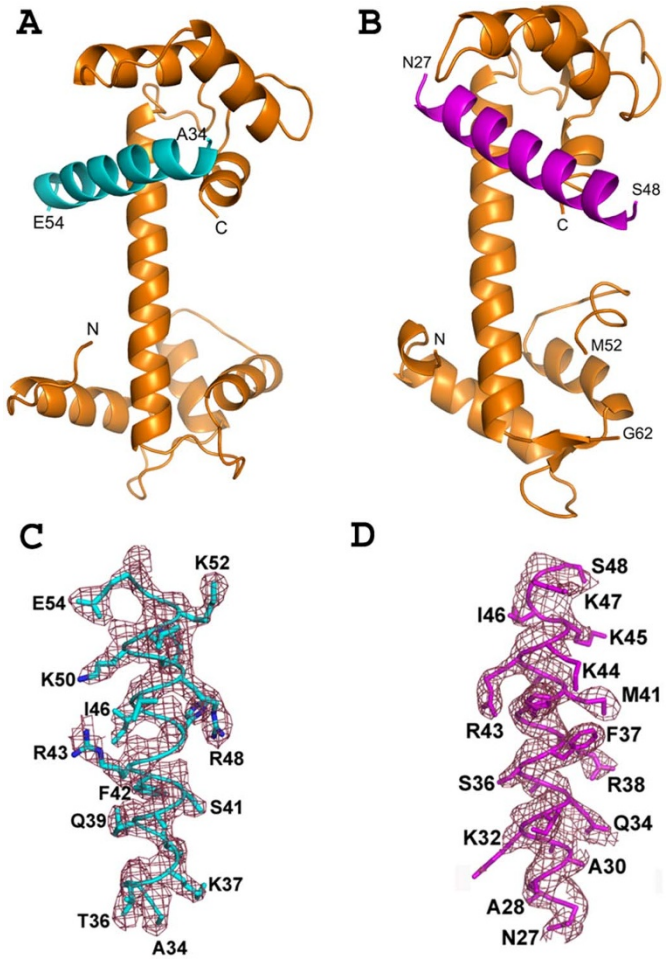

Figure 3 | Cartoon representations of the structure of (A) *apo* CaM-$(Gly)_5$-NmIQ and (B) *apo* CaM-$(Gly)_5$-NgIQ complexes, with CaM (orange), NmIQ (cyan) and NgIQ (magenta). N and C-termini are labeled. *2Fo-Fc* electron density maps of (C) NmIQ and (D) NgIQ peptides. Maps are contoured at a level of 1σ.

might not be possible because of the length of the linker. In these types of situations, the linked partners will instead engage in an intermolecular interaction[38] to retain its natural binding. Such intermolecular interactions (i.e. peptide and protein interactions with adjacent molecules) were observed in the case of CaM and Neurogranin (Ng) IQ motif peptide. For the CaM-$(Gly)_5$-NmIQ complex, the peptide interacts through an intramolecular fashion. In both cases, the IQ peptides interact with the C-lobe of CaM. When the structure of CaM-$(Gly)_5$-NmIQ and CaM-$(Gly)_5$-NgIQ are superimposed, the bound IQ peptides are in opposite directions (Figure 5). This mode of binding is essential to keep the critical PKC phosphorylation target Ser41 (of Nm) and Ser36 (of Ng) in the negatively charged pocket. Similarly, this mode of binding also preserves the critical Arg43 (of Nm) and Arg38 (of Ng) in its specific binding pocket to retain 11 and 5 hydrogen bonding contacts with CaM for Nm and Ng, respectively. Functional studies with unlinked full-length proteins support the observed unique mode of binding of Ng and Nm with CaM as natural binding.

Previously, we reported that Ng enhances postsynaptic sensitivity and increases synaptic strength in an activity- and NMDAR-dependent manner[19]. Further Ng-mediated potentiation of synaptic transmission mimics and occludes long-term potentiation (LTP). Expression of Ng mutants that lack the ability to bind to, or dissociate from CaM, fails to potentiate synaptic transmission, and this strongly suggests that regulated Ng–CaM binding is necessary for Ng-mediated potentiation. Moreover, reduced expression of Ng will block LTP induction. We have established that the Ng–CaM interaction can provide a mechanistic link between the induction and expression of postsynaptic potentiation[19]. The crystal structure shows that the Arg38 of Ng makes strong H-bond contacts with CaM, and the ITC experiment shows that the mutant Ng (Arg38Ala) does not bind to the *apo* CaM. Through electrophysiological experiments, we found that mutant Ng (Arg38Ala) fails to potentiate synaptic transmission (Figure 6), further supporting the importance of Ng-CaM interaction in Ng-mediated enhancement of synaptic strength.

Nm and Ng are unstructured under physiological *in vitro* conditions. In general, the intracellular axoplasm environment is highly crowded (300 mg/ml), harboring an intricate and complex network of biological macromolecules[39]. Previously, the in cell NMR studies showed that many proteins, which are unstructured under *in vitro*

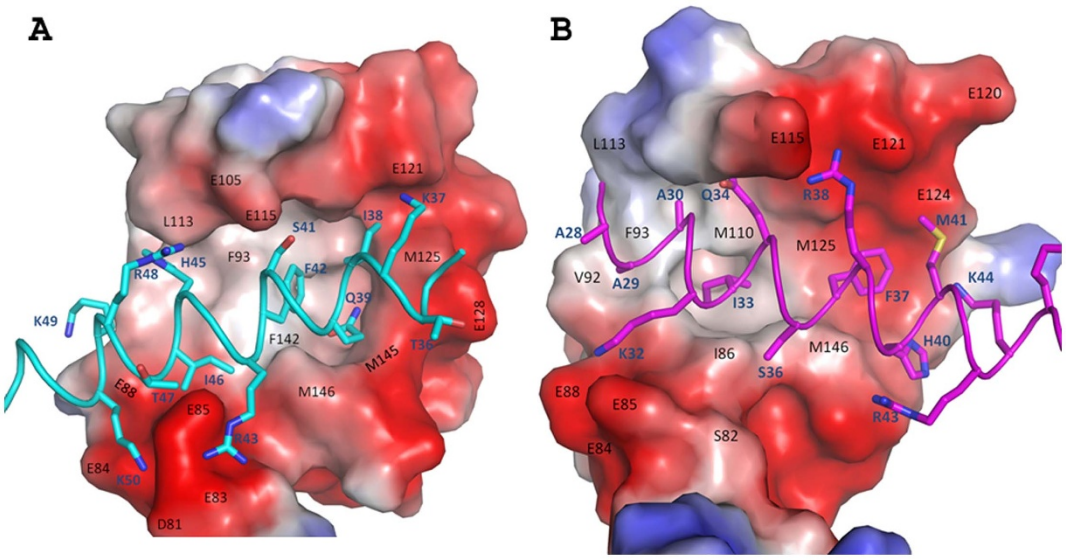

Figure 4 | Interactions of (A) NmIQ and (B) NgIQ peptides with the C-lobe of CaM. CaM is shown in surface representation and key side chains of IQ peptides involved in interactions are shown as sticks. The electrostatic surface potential of C-lobes of CaM are shown (negative charge, red; positive charge, blue).

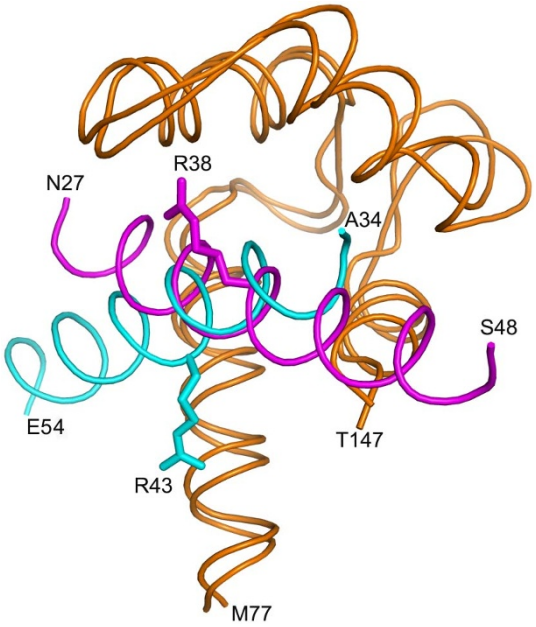

Figure 5 | Superposition of the structures of NmIQ (cyan) and NgIQ (magenta) bound to C-lobe of *apo* CaM (orange). Side chains of Arg43 of Nm and Arg38 of Ng are shown as sticks.

conditions, are well folded inside the cell[40,41]. A similar study might help to understand the nature of Ng and Nm inside the cells.

In summary, this is the first report of the crystal structure of the intrinsically unstructured, neuron-specific substrate proteins, Nm/Ng, as IQ peptides in complex with CaM. The unstructured IQ peptides (24 aa) interact with the C-lobe of CaM and gain an α-helical conformation. Biophysical studies with full-length Nm/Ng confirmed their unstructured properties in solution. Further, ITC studies revealed that full-length Nm/Ng, their mutants, and their IQ peptides bind stronger to the *apo* CaM than to Ca^{2+}/CaM. The functional relevance of the identified key residue Arg38 in Ng-mediated synaptic function was verified, with functional data showing that the Ng mutant (Arg38Ala) is incapable of enhancing synaptic strength. This study provides the structural basis for the association of Nm/Ng with CaM, a crucial interaction for several learning- and memory-associated functions in neuronal cells.

Methods

Expression, purification and characterization of Nm and Ng. Full-length Nm (accession no NP_032109) and Ng (accession no NP_071312) proteins were expressed in *E. coli BL21 (DE3)* cells harboring respective genes in pQE30 (Qiagen, USA) plasmids. *E. coli* cells were cultured in 1 L LB media (supplemented with 100 μg/mL ampicillin) at 37°C until the OD_{600} reached between 0.6–0.8 AU. The culture was then maintained at 16°C before protein expression was induced with 0.15 mM IPTG. Cells were grown for 16 h at 16°C, and harvested by centrifugation at 9800 g for 10 min. Cell pellets from 2 L cell culture were resuspended in 100 ml lysis buffer (50 mM Tris-HCl (pH-8.0), 500 mM NaCl, 10% v/v glycerol, 20 mM imidazole, 20 mM BME and 0.1 mM PMSF). After sonication, the cell lysate was centrifuged at 39,000 g for 30 min. The supernatant was mixed with 5 ml of Ni–NTA (Qiagen, USA), and washed thrice using 30 ml of lysis buffer. The protein was released from the Ni-NTA resin using 10 ml of lysis buffer supplemented with 300 mM imidazole. The protein was then passed through a HiLoad™ 16/60 Superdex™ 200 prep grade (Amersham Biosciences, Sweden) gel filtration column and eluted in a buffer consisting of 50 mM $NaH_2PO_4.2H_2O$ (pH 7.4), 300 mM NaCl, 20 mM BME, and 0.1% Triton X100. The mean stokes radius and apparent molecular weight of Nm and Ng were calculated using standard curves (Supplementary figure 1B and 1C) generated based on the elution volumes of proteins of known molecular weight and stokes radius[42]. Dynamic Light Scattering (Protein solutions, USA) and Circular Dichroism (JASCO J-175, Japan) experiments were performed in the same buffer. ^{1}H NMR experiments were performed with full-length proteins in 50 mM sodium phosphate (pH 7.4), 100 mM NaCl and 95% H_2O plus 5% D_2O at 25°C with 16 K data point. The concentration of both proteins was 0.2 mM. Suppression of the water resonance was achieved through the WATERGATE technique.

Based on the complex structures, various point mutations on full-length Nm, Ng and CaM were introduced using inverse PCR (Table 1) and mutant proteins were purified as described above.

Cloning, expression and purification of CaM constructs. NmIQ (34–57) and NgIQ (27–50) motifs were linked to the C-terminus of CaM *via* a 5-glycine flexible linker (CaM-$(Gly)_5$-NmIQ and CaM-$(Gly)_5$-NgIQ) using a three-step fusion PCR procedure, as described by Ye *et al.*[30]. The final PCR product was digested with Nde1 and Xho1 restriction enzymes (New England Biolabs, UK) along with the pGS21a vector (GeneScript, USA). Predigested CaM-$(Gly)_5$-NmIQ and CaM-$(Gly)_5$-NgIQ genes and pGS21a vector were ligated, transformed into chemically competent *E. coli DH5α* cells and screened for positive colony formation. The CaM-$(Gly)_5$-NmIQ and CaM-$(Gly)_5$-NgIQ gene sequences were verified by DNA sequencing.

For protein expression, the recombinant plasmids (pGS21a- CaM-$(Gly)_5$-NmIQ and pGS21a- CaM-$(Gly)_5$-NgIQ) were transformed into *E. coli BL21 (DE3)* chemically competent cell and plated onto agar plates. A single colony was used to inoculate 100 ml of the LB media containing 100 μg/ml ampicillin. The expression and purification strategy was similar to that of full-length Nm/Ng described above, with the exception that the proteins were passed through HiLoad™ 16/60 Superdex™ 75 prep grade columns (Amersham Biosciences, Sweden) and eluted with a buffer consisting of 20 mM Imidazole pH 8.0, 100 mM NaCl, 2 mM EGTA (buffer A).

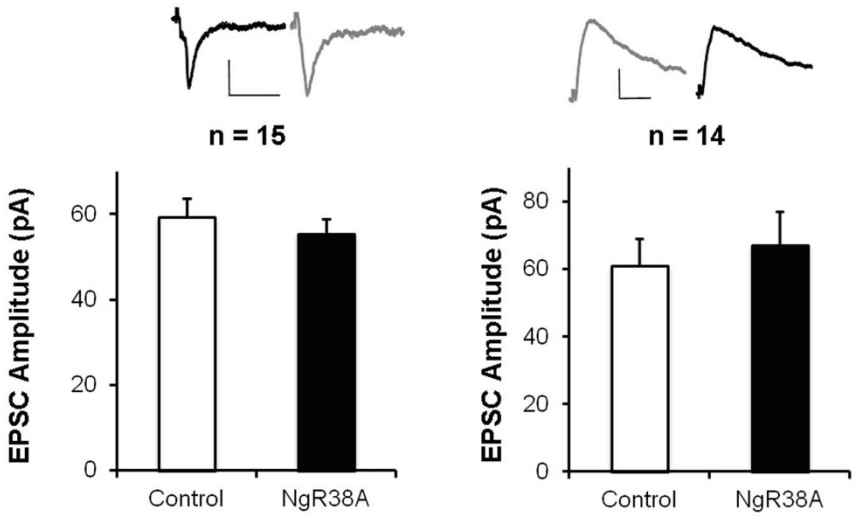

Figure 6 | NgR38A does not enhance AMPAR-mediated synaptic transmission. *Inset*, sample traces of evoked AMPAR (left)- and NMDAR(right)-mediated synaptic responses recorded at −60 mV (the peak amplitude) and +40 mV (the amplitude at 60 ms latency, when AMPAR responses are decayed), respectively. *Scale bars*, 20 pA, 40 ms. *Left graph*, comparisons of evoked AMPAR-mediated responses from NgR38A-infected and control neurons. *Right graph*, simultaneous recordings of evoked NMDAR-mediated responses from NgR38A-infected and control neurons.

A similar expression and purification procedure was adopted for $(His)_6$-tagged CaM (accession no NP_033920) from pETDuet-1 vector (Novagen, USA). CaM protein was eluted from gel filtration column in either buffer A or a buffer containing 20 mM HEPES (pH 8.0), 100 mM NaCl and 10 mM $CaCl_2$ (buffer B) to elute *apo* CaM or Ca^{2+}/CaM, respectively. For SeMet SAD phasing, selenomethionine-labeled proteins were produced using LeMaster media[43] following a similar procedure as described above. All protein purification steps were carried out at 4°C unless otherwise indicated.

Isothermal titration calorimetry. Isothermal titration calorimetry was used to study the binding of full-length wild type Nm/Ng proteins, full-length mutant Nm/Ng proteins and their synthetic wild-type IQ motif peptides (Nm (NmIQ: aa34–57) and Ng (NgIQ: aa27–50)) (Table 1) with Ca^{2+}/CaM (in buffer B), *apo* CaM and mutant CaM (both in buffer A). ITC experiments were performed using either VP-ITC or iTC200 calorimeter (indicated in brackets) (Microcal, LLC) at room temperature (24°C) with 0.3 (or 0.04) ml of Ca^{2+}/CaM or *apo* CaM in the injector cell, and 1.4 (or 0.2) ml of Nm/NmIQ or Ng/NgIQ in the sample cell, respectively. Samples were thoroughly degassed and centrifuged to remove precipitates. All experiments used 10 (or 2) µl volumes per injection. Two consecutive injections were separated by 5 (or 2) min to allow the peak to return to baseline. Data from control experiments, i.e., titration of protein/peptides into buffer, were subtracted from each experiment to compensate for the heat of dilution. ITC data were analyzed with a single-site fitting model using Origin 7.0 software (OriginLab Corp. MA, USA).

Crystallization and structure determination. Crystallization trails for *apo* CaM-$(Gly)_5$-NmIQ and *apo* CaM-$(Gly)_5$-NgIQ complexes were performed with a protein concentration of 10–12 mg/ml using the hanging drop vapor diffusion method at room temperature. The initially identified conditions from Hampton Research (Aliso Viejo, CA, USA) and Qiagen (Valencia, CA, USA) were further optimized. Best crystals of *apo* CaM-$(Gly)_5$-NmIQ complex crystals were obtained from a condition consisting of 0.12 mM MgAcO, 8% PEG 3350 and 10% EtOH. Similarly, the *apo* CaM-$(Gly)_5$-NgIQ complex crystals were obtained using a condition consisting of 0.1 M imidazole (pH 8.0) and 1.2 M sodium citrate tribasic dihydrate. Where necessary, crystals were cryo-protected with reservoir condition supplemented with 10% glycerol and flash-cooled in N_2 cold stream at 100 K.

The molecular replacement method did not yield any structure solution, which led us to collect the Single wavelength Anomalous Dispersion (SAD) data sets in the synchrotron beam line X8C (NSLS, Brookhaven National Laboratory) and 13B1 SW6 (National Synchrotron Radiation Research Center (NSRRC), Taiwan) using a Quantum 4-CCD detector (Area Detector Systems Corp Poway, CA, USA). All data sets were processed using HKL2000[44]. Heavy atom (Se) location, phasing and density modification were performed using the program ShelxC/D/E[45], and model building was carried out with the program Buccaneer[46] in CCP4. Where necessary, the model was manually built in COOT[47] and twin refinement was carried out in Refmac5[48]. At the final stage of refinement, well-ordered water molecules were included. The models have good stereochemistry, as analyzed by PROCHECK[49] (Table 2). All structure-related figures reported in this manuscript were generated using PyMol[50].

Animals and hippocampal slice preparation. Young Sprague-Dawley rats (postnatal day 5 or 6) were purchased from Charles River Laboratories (Portage, MI, USA) and maintained on a daily 12 h light:dark cycle. All biosafety procedures and animal care protocols were approved by the Medical College of Wisconsin Institutional Animal Care and Use Committee (IACUC). Hippocampal slices were prepared as described previously[51].

Electrophysiology. Simultaneous whole-cell double recordings were obtained for nearby pairs of infected (fluorescent) and uninfected (non-fluorescent) neurons under visual guidance using differential interference contrast illumination as previously described[19,52]. Two bipolar electrodes (2-contact; FHC, Bowdoin, ME, USA) were placed on the Schaffer collateral fibers between 300 and 500 mm from the recorded cells to evoke synaptic responses. Responses obtained from the two stimulating electrodes were averaged for each cell and counted as an 'n' of 1. The recording chamber was perfused with (in mM): NaCl, 119; KCl, 2.5; $CaCl_2$, 4; $MgCl_2$, 4: $NaHCO_3$, 26; NaH_2PO_4, 1; glucose, 11; picrotoxin, 0.1; 2-chloroadenosine, 2 µM; at pH 7.4; and gassed with 5% CO_2, 95% O_2. Patch recording pipettes (3-6 MΩ) were filled with (in mM): cesium methanesulfonate, 115; CsCl, 20; HEPES, 10; $MgCl_2$, 2.5; Na_2ATP, 4; Na_3GTP, 0.4; sodium phosphocreatine, 10; EGTA, 0.6; at pH 7.25. Voltage-clamp whole-cell recordings were acquired with a Multiclamp 700A amplifier (Axon Instruments, Sunnyvale, CA, USA).

Statistical analysis. Comparison of electrophysiological responses between pairs of infected and uninfected neurons was carried out using the paired non-parametric Wilcoxon test.

Protein data bank accession code. Coordinates and structure factors of *apo* CaM-$(Gly)_5$-NmIQ and *apo* CaM-$(Gly)_5$-NgIQ have been deposited with RCSB Protein Data Bank with codes 4E53 and 4E50, respectively.

1. Andreasen, T. J., Luetje, C. W., Heideman, W. & Storm, D. R. Purification of a novel calmodulin binding protein from bovine cerebral cortex membranes. *Biochemistry* **22**, 4615–8 (1983).
2. Neuner-Jehle, M., Denizot, J. P. & Mallet, J. Neurogranin is locally concentrated in rat cortical and hippocampal neurons. *Brain research* **733**, 149–54 (1996).
3. Clayton, D. F., George, J. M., Mello, C. V. & Siepka, S. M. Conservation and expression of IQ-domain-containing calpacitin gene products (neuromodulin/GAP-43, neurogranin/RC3) in the adult and developing oscine song control system. *Developmental neurobiology* **69**, 124–40 (2009).
4. Xia, Z. & Storm, D. R. The role of calmodulin as a signal integrator for synaptic plasticity. *Nat Rev Neurosci* **6**, 267–76 (2005).
5. Shen, Y., Mani, S., Donovan, S. L., Schwob, J. E. & Meiri, K. F. Growth-associated protein-43 is required for commissural axon guidance in the developing vertebrate nervous system. *J Neurosci* **22**, 239–47 (2002).
6. Denny, J. B. Molecular mechanisms, biological actions, and neuropharmacology of the growth-associated protein GAP-43. *Curr Neuropharmacol* **4**, 293–304 (2006).
7. Nelson, R. B. & Routtenberg, A. Characterization of protein F1 (47 kDa, 4.5 pI): a kinase C substrate directly related to neural plasticity. *Exp Neurol* **89**, 213–24 (1985).
8. Hulo, S., Alberi, S., Laux, T., Muller, D. & Caroni, P. A point mutant of GAP-43 induces enhanced short-term and long-term hippocampal plasticity. *Eur J Neurosci* **15**, 1976–82 (2002).
9. Routtenberg, A., Cantallops, I., Zaffuto, S., Serrano, P. & Namgung, U. Enhanced learning after genetic overexpression of a brain growth protein. *Proc Natl Acad Sci U S A* **97**, 7657–62 (2000).
10. Holahan, M. & Routtenberg, A. The protein kinase C phosphorylation site on GAP-43 differentially regulates information storage. *Hippocampus* **18**, 1099–102 (2008).
11. Bernal, J., Rodriguez-Pena, A., Iniguez, M. A., Ibarrola, N. & Munoz, A. Influence of thyroid hormone on brain gene expression. *Acta medica Austriaca* **19 Suppl 1**, 32–5 (1992).
12. Husson, M. *et al.* Triiodothyronine administration reverses vitamin A deficiency-related hypo-expression of retinoic acid and triiodothyronine nuclear receptors and of neurogranin in rat brain. *The British journal of nutrition* **90**, 191–8 (2003).
13. Alvarez-Bolado, G., Rodriguez-Sanchez, P., Tejero-Diez, P., Fairen, A. & Diez-Guerra, F. J. Neurogranin in the development of the rat telencephalon. *Neuroscience* **73**, 565–80 (1996).
14. Pak, J. H. *et al.* Involvement of neurogranin in the modulation of calcium/calmodulin-dependent protein kinase II, synaptic plasticity, and spatial learning: a study with knockout mice. *Proceedings of the National Academy of Sciences of the United States of America* **97**, 11232-7 (2000).
15. Dominguez-Gonzalez, I., Vazquez-Cuesta, S. N., Algaba, A. & Diez-Guerra, F. J. Neurogranin binds to phosphatidic acid and associates to cellular membranes. *The Biochemical journal* **404**, 31–43 (2007).
16. Diez-Guerra, F. J. Neurogranin, a link between calcium/calmodulin and protein kinase C signaling in synaptic plasticity. *IUBMB Life* **62**, 597–606 (2010).
17. Zhabotinsky, A. M., Camp, R. N., Epstein, I. R. & Lisman, J. E. Role of the neurogranin concentrated in spines in the induction of long-term potentiation. *Journal of Neuroscience* **26**, 7337–47 (2006).
18. Zhong, L. & Gerges, N. Z. Neurogranin and synaptic plasticity balance. *Commun Integr Biol* **3**, 340–2 (2010).
19. Zhong, L., Cherry, T., Bies, C. E., Florence, M. A. & Gerges, N. Z. Neurogranin enhances synaptic strength through its interaction with calmodulin. *The EMBO journal* **28**, 3027–39 (2009).
20. Ran, X., Miao, H. H., Sheu, F. S. & Yang, D. Structural and dynamic characterization of a neuron-specific protein kinase C substrate, neurogranin. *Biochemistry* **42**, 5143–50 (2003).
21. Chapman, E. R., Au, D., Alexander, K. A., Nicolson, T. A. & Storm, D. R. Characterization of the calmodulin binding domain of neuromodulin. Functional significance of serine 41 and phenylalanine 42. *J Biol Chem* **266**, 207–13 (1991).
22. Alexander, K. A., Wakim, B. T., Doyle, G. S., Walsh, K. A. & Storm, D. R. Identification and characterization of the calmodulin-binding domain of neuromodulin, a neurospecific calmodulin-binding protein. *The Journal of biological chemistry* **263**, 7544–9 (1988).
23. Prichard, L., Deloulme, J. C. & Storm, D. R. Interactions between neurogranin and calmodulin in vivo. *J Biol Chem* **274**, 7689–94 (1999).
24. Huang, K. P., Huang, F. L. & Chen, H. C. Characterization of a 7.5-kDa protein kinase C substrate (RC3 protein, neurogranin) from rat brain. *Archives of biochemistry and biophysics* **305**, 570–80 (1993).
25. Uversky, V. N. Natively unfolded proteins: a point where biology waits for physics. *Protein science : a publication of the Protein Society* **11**, 739–56 (2002).
26. Rehm, T., Huber, R. & Holak, T. A. Application of NMR in structural proteomics: screening for proteins amenable to structural analysis. *Structure* **10**, 1613–8 (2002).
27. Permyakov, S. E., Millett, I. S., Doniach, S., Permyakov, E. A. & Uversky, V. N. Natively unfolded C-terminal domain of caldesmon remains substantially unstructured after the effective binding to calmodulin. *Proteins* **53**, 855–62 (2003).
28. Kleerekoper, Q. K. & Putkey, J. A. PEP-19, an intrinsically disordered regulator of calmodulin signaling. *The Journal of biological chemistry* **284**, 7455–64 (2009).
29. De Guzman, R. N., Martinez-Yamout, M. A., Dyson, H. J. & Wright, P. E. Interaction of the TAZ1 domain of the CREB-binding protein with the activation domain of CITED2: regulation by competition between intrinsically unstructured

ligands for non-identical binding sites. *The Journal of biological chemistry* **279**, 3042–9 (2004).
30. Ye, Q., Li, X., Wong, A., Wei, Q. & Jia, Z. Structure of calmodulin bound to a calcineurin peptide: a new way of making an old binding mode. *Biochemistry* **45**, 738–45 (2006).
31. Osawa, M. *et al.* A novel target recognition revealed by calmodulin in complex with Ca2+-calmodulin-dependent kinase kinase. *Nat Struct Biol* **6**, 819–24 (1999).
32. Lo, D. C., McAllister, A. K. & Katz, L. C. Neuronal transfection in brain slices using particle-mediated gene transfer. *Neuron* **13**, 1263–8 (1994).
33. Gerendasy, D. Homeostatic tuning of Ca2+ signal transduction by members of the calpacitin protein family. *Journal of neuroscience research* **58**, 107–19 (1999).
34. Han, N. L. *et al.* Proteomics analysis of the expression of neurogranin in murine neuroblastoma (Neuro-2a) cells reveals its involvement for cell differentiation. *Int J Biol Sci* **3**, 263–73 (2007).
35. Meiri, K. F., Hammang, J. P., Dent, E. W. & Baetge, E. E. Mutagenesis of ser41 to ala inhibits the association of GAP-43 with the membrane skeleton of GAP-43-deficient PC12B cells: effects on cell adhesion and the composition of neurite cytoskeleton and membrane. *Journal of neurobiology* **29**, 213–32 (1996).
36. Pfuhl, M., Al-Sarayreh, S. & El-Mezgueldi, M. The calponin regulatory region is intrinsically unstructured: novel insight into actin-calponin and calmodulin-calponin interfaces using NMR spectroscopy. *Biophysical journal* **100**, 1718–28 (2011).
37. Houdusse, A. *et al.* Crystal structure of apo-calmodulin bound to the first two IQ motifs of myosin V reveals essential recognition features. *Proceedings of the National Academy of Sciences of the United States of America* **103**, 19326–31 (2006).
38. Kingston, R. L., Baase, W. A. & Gay, L. S. Characterization of nucleocapsid binding by the measles virus and mumps virus phosphoproteins. *J Virol* **78**, 8630–40 (2004).
39. Ellis, R. J. Macromolecular crowding: obvious but underappreciated. *Trends in biochemical sciences* **26**, 597–604 (2001).
40. Rivas, G., Ferrone, F. & Herzfeld, J. Life in a crowded world. *EMBO reports* **5**, 23–7 (2004).
41. Dedmon, M. M., Patel, C. N., Young, G. B. & Pielak, G. J. FlgM gains structure in living cells. *Proceedings of the National Academy of Sciences of the United States of America* **99**, 12681–4 (2002).
42. le Maire, M., Ghazi, A., Moller, J. V. & Aggerbeck, L. P. The use of gel chromatography for the determination of sizes and relative molecular masses of proteins. Interpretation of calibration curves in terms of gel-pore-size distribution. *The Biochemical journal* **243**, 399–404 (1987).
43. Hendrickson, W. A., Horton, J. R. & LeMaster, D. M. Selenomethionyl proteins produced for analysis by multiwavelength anomalous diffraction (MAD): a vehicle for direct determination of three-dimensional structure. *EMBO J* **9**, 1665–72 (1990).
44. Otwinowski, Z. & Minor, W. Processing of X-ray diffraction data collected in oscillation mode. *Macromolecular Crystallography, Pt A* **276**, 307–326 (1997).
45. Sheldrick, G. M. A short history of SHELX. *Acta Crystallogr A* **64**, 112–22 (2008).
46. Cowtan, K. The Buccaneer software for automated model building. 1. Tracing protein chains. *Acta Crystallogr D Biol Crystallogr* **62**, 1002–11 (2006).
47. Emsley, P. & Cowtan, K. Coot: model-building tools for molecular graphics. *Acta Crystallogr D Biol Crystallogr* **60**, 2126–32 (2004).
48. Vagin, A. A. *et al.* REFMAC5 dictionary: organization of prior chemical knowledge and guidelines for its use. *Acta Crystallogr D Biol Crystallogr* **60**, 2184–95 (2004).
49. Laskowski, R. A., Macarthur, M. W., Moss, D. S. & Thornton, J. M. Procheck - a Program to Check the Stereochemical Quality of Protein Structures. *Journal of Applied Crystallography* **26**, 283–291 (1993).
50. DeLano, W. L. & Lam, J. W. PyMOL: A communications tool for computational models. *Abstracts of Papers of the American Chemical Society* **230**, U1371–U1372 (2005).
51. Gahwiler, B. H., Capogna, M., Debanne, D., McKinney, R. A. & Thompson, S. M. Organotypic slice cultures: a technique has come of age. *Trends in Neurosciences* **20**, 471–7 (1997).
52. Zhong, L., Kaleka, K. S. & Gerges, N. Z. Neurogranin phosphorylation fine-tunes long-term potentiation. *The European journal of neuroscience* **33**, 244–50 (2011).

Acknowledgements

We are grateful to the Biomedical Research Council of Singapore (BMRC), A*STAR, (R154000461305) and AcRF (Tier 1) National University of Singapore (NUS), for the partial support of this study. NZG was supported by grants from US National Institute on Aging (AG032320) and Alzheimer's Association. FWS was supported by Ministry of Education, Singapore (R-154-000-228-112). X-ray diffraction data for this study were measured at beamline 13B1 of National Synchrotron Radiation Research Centre (NSRRC), Taiwan, and BNL New York, USA. We also acknowledge Yi-Hui Chen from NSRRC for her assistance during data collection. Veerendra Kumar is a graduate scholar in receipt of a research scholarship from the NUS and from R-154-000-228-112.
We declare that none of the authors have a financial interest related to this work.

Author contributions

J.S. and F.S.S. conceived of the study. V.K. carried out crystallographic and biophysical experiments. J.S. and J.Se analyzed the X-ray data. V.P.R.C. and X.T. performed mutations. V.P.R.C., X.T. and V.K. performed ITC experiments. A.V.C. analyzed the ITC data. L.Z. and N.Z.G. performed and analyzed electrophysiology experiments. V.K. and J.S. wrote the manuscript.

Additional information

Supplementary information accompanies this paper at http://www.nature.com/scientificreports

Competing financial interests: The authors declare no competing financial interests.

How to cite this article: Kumar, V. *et al.* Structural Basis for the Interaction of Unstructured Neuron Specific Substrates Neuromodulin and Neurogranin with Calmodulin. *Sci. Rep.* **3**, 1392; DOI:10.1038/srep01392 (2013).